



CISM COURSES AND LECTURES NO. 478  
INTERNATIONAL CENTRE FOR MECHANICAL SCIENCES

---

# MICROSYSTEMS MECHANICAL DESIGN

EDITED BY

FRANCESCO DE BONA  
ENIKO T. ENIKOV

 SpringerWienNewYork

# **CISM COURSES AND LECTURES**

Series Editors:

The Rectors

Giulio Maier - Milan  
Jean Salençon - Palaiseau  
Wilhelm Schneider - Wien

The Secretary General

Bernhard Schrefler - Padua

Executive Editor

Paolo Serafini - Udine

The series presents lecture notes, monographs, edited works and proceedings in the field of Mechanics, Engineering, Computer Science and Applied Mathematics.

Purpose of the series is to make known in the international scientific and technical community results obtained in some of the activities organized by CISM, the International Centre for Mechanical Sciences.

INTERNATIONAL CENTRE FOR MECHANICAL SCIENCES

COURSES AND LECTURES - No. 478



# MICROSYSTEMS MECHANICAL DESIGN

EDITED BY

FRANCESCO DE BONA  
UNIVERSITY OF UDINE, ITALY

ENIKO T. ENIKOV  
UNIVERSITY OF ARIZONA, USA

SpringerWienNewYork

The publication of this volume was co-sponsored and co-financed by the UNESCO Venice Office - Regional Bureau for Science in Europe (ROSTE) and its content corresponds to a CISM Advanced Course supported by the same UNESCO Regional Bureau.

This volume contains 172 illustrations

This work is subject to copyright.  
All rights are reserved,  
whether the whole or part of the material is concerned  
specifically those of translation, reprinting, re-use of illustrations,  
broadcasting, reproduction by photocopying machine  
or similar means, and storage in data banks.  
© 2006 by CISM, Udine  
Printed in Italy  
SPIN 11817536

In order to make this volume available as economically and as rapidly as possible the authors' typescripts have been reproduced in their original forms. This method unfortunately has its typographical limitations but it is hoped that they in no way distract the reader.

ISBN-10 3-211-37453-1 SpringerWienNewYork  
ISBN-13 978-3-211-37453-5 SpringerWienNewYork

## **PREFACE**

Nowadays, micromechanics (i.e., mechanics of microsystems) is probably one of the most promising and rapidly growing fields among new emerging technologies. In fact, the possibility of reducing the size of mechanical structures to the micro-domain opens a wide variety of possible applications in the biomedical, aeronautical, and automotive fields, in robotics, in molecular engineering, in fiber optics, and in fluidics technology. One of the main aspects that slows down the development of innovative industrial products based on microsystem technology is the existing lack of engineering tools to allow a reliable design of microsystems .

The aim of this book is that of collecting the texts of the lectures given at the CISM course on: *Microsystems Mechanical Design*, held in July 2004.

The purpose of this course was to introduce the basic tools used in the mechanical design of microsystems, the fabrication methods for these systems, and several applications of this technology. The links between micro- and nanotechnologies were also discussed and light was shed on the potential applications of microsystems to nano-scale manipulation of matter, thus introducing the topic of nano-scale engineering mechanics, which will be fully explored in a future course.

This book is arranged in 8 sections. In the first section an introduction on microsystems and the techniques for their fabrication will be presented, with a thorough description of surface and bulk micromachining techniques and of other microfabrication processes as LIGA and anodizing bonding.

In the next three sections the case of microsystems loaded electrostatically is considered. In particular scale effects are discussed, the static and the dynamic behaviors of a single degree of freedom electromechanical microsystem are considered; an extension to multi-degree of freedom system is also proposed with the aim analyzing the case of continuum structures discretised with FEM and BEM techniques. The case of a cantilever beam loaded electrostatically was finally considered and an overview of the main analytical and numerical solutions available in literature is proposed.

As an example of application, in the fifth section the design case of a microactuator with integrated position sensor was considered, particularly concerning structural and thermal analysis and also the electrical circuit design to achieve the capacitive readout of position.

A section is then dedicated to micro and nano assembly; different microassembly technique and devices as mechanical and vacuum grippers, electrostatic and magnetic manipulation approach are discussed. New emerging nanoassembly techniques based on charge writing, and liquid phase and gas phase assembly of nanoparticles are also presented

Compliant microstructures are widely used in the design of microsystems. A broad overview of the topics related to the mechanical design of compliant micromechanisms

*is thus presented in the next section. Design methodologies to be used in the design of devices based on leaf springs, flexural notches and continuum structures with distributed compliance are given, and a critical presentation of the peculiarities of these solutions is provided.*

*In the last section the basic concepts related to the newly emerging field of microfluidics are presented. Following a brief introduction of the general conservation and particular laws, three size effects are introduced. The velocity slip boundary condition for gas flows as well as the electrokinetic and polar-mechanics effects for liquid flow in microdomains are introduced. Pressure-driven gas flows and electrokinetically-driven liquid flows in microchannels are analyzed in details. Finally, several flow diagnostic techniques and fabrication of microfluidic systems are described.*

*In conclusion we thank Professors Velarde and Stepan for their aid and encouragement in the organization of the workshop. We wish also to thank Ms. P. Agnola and all the local organizers in Udine for their hospitality and help in organizing this course.*

*Eniko T. Enikov  
Francesco De Bona*

## CONTENTS

### Preface

Introduction to Micro-Systems and to the Techniques for Their Fabrication <i>by E.T. Enikov</i> .....	1
Microstructures Under Electrostatic Loads: Discrete System Modelling <i>by F. De Bona</i> .....	37
Dynamics of Mechatronic Systems at Microscale <i>by E. Brusa</i> .....	57
Continuum Microstructures Loaded Electrostatically <i>by F. De Bona, M. Gh. Munteanu</i> .....	81
Design of Electro-Thermal Micro-Positioners: Mechanics and Electronic Position Detection <i>by K.V. Lazarov E.T. Enikov</i> .....	101
Design of Compliant Micromechanisms <i>by F. De Bona, S. Zelenika</i> .....	119
Micro and Nano Assembly and Manipulation Techniques for MEMS <i>by E.T. Enikov</i> .....	135
Microfluidics: Device Science and Technology <i>By Lap Man Lee, Luthur Siu Lun Cheung and Yitshak Zohar</i> .....	157

# Introduction to Micro-Systems and to the Techniques for Their Fabrication

Eniko T. Enikov

Department of Aerospace and Mechanical Engineering, University of Arizona, Tucson, AZ, USA

**Abstract** This chapter presents an introduction to the main manufacturing processes for micro-systems. After a brief historical overview of the field of micro-systems, their main manufacturing techniques are reviewed. These include substrate preparation, photolithography, oxidation and diffusion, thin-film deposition, and wet and dry etching techniques. MEMS-specific processes including bulk- and surface-micromachining, LIGA, soft-lithography, and anodic bonding are also presented. The material is illustrated with multiple examples of process parameter calculation. Examples of MEMS devices fabricated in the laboratory of the author are also provided.

## 1 Definition of Micro-Electromechanical Systems

The term micro-electromechanical systems (MEMS) was coined to describe a sub-millimeter integrated electro-mechanical system that contains both electrical and mechanical components with sizes in the range of 1  $\mu\text{m}$  to 1 mm and is fabricated in a massively parallel manner through photolithography. Initially these were simple electrostatically driven cantilevers, fabricated using semiconductor processing techniques (Peterson, 1982). A defining feature of MEMS is their massively parallel manufacture, which results from the use of photolithographic tools for their fabrication. As a result, large quantities of identical planar devices can be made at a very low unit-cost. Another important consequence of the use of photolithography is that the smallest feature producible with this technology has a characteristic dimension roughly equal to the wavelength of light (250-300 nm for UV systems). With the advance of exposure systems that now operate in deep UV, or use even shorter wavelengths such as e-beam lithography and x-ray lithography, the lowest size limit is constantly being broken and currently structures in the 30-100 nm range are possible. Figure 1 illustrates the size definition of MEMS in comparison with other commonly known structures and technologies.

## 2 Brief History of Micro-Electromechanical Systems

The technological origins of MEMS devices can be traced back to 1947, when the first semiconductor transistor was invented in Bell Telephone Laboratories. Approximately

<b>Physical Examples</b>	atom 1Å	quantum dots 1nm	wavelength of light	biological cells 1µm	insects 1mm	humans 1cm	1m	10m
<b>Terminology</b>	Nano-technology			<b>MEMS</b>		Conventional Mechatronic Systems		

**Figure 1.** The scale of micro devices.

ten years later the first integrated circuit using a Ge sliver attached to a glass slide was demonstrated by Kilby (1964) of Texas Instruments (see Fig. 2).

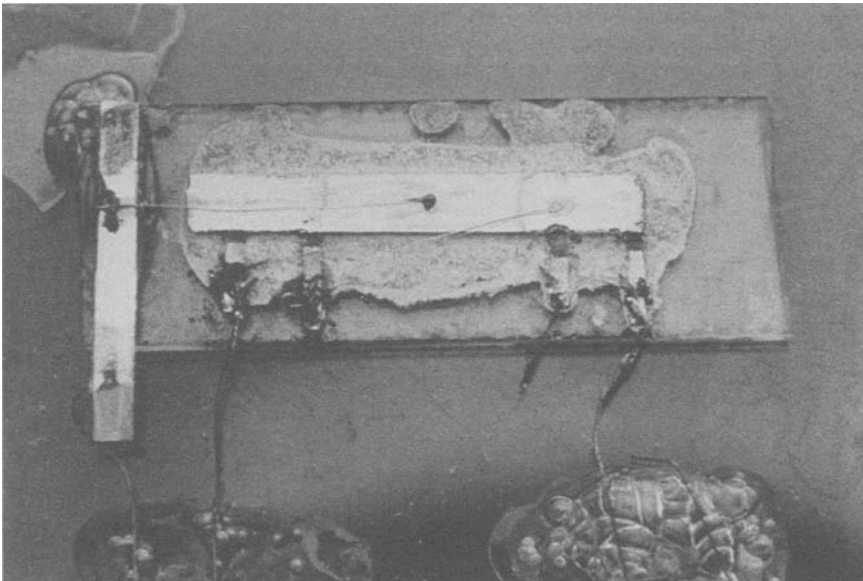


**Figure 2.** First Integrated Circuit. Courtesy of Texas Instruments

Soon, Robert Noyce of Fairchild Semiconductor announced the development of a planar process capable of integrating multiple transistors and resistors on a single Si substrate, which led to a technological revolution in the electronic industry. Since the 1970s the number of integrated components per unit area has doubled every two to three years, a phenomenon dubbed Moore's law. Elements of micro-electromechanical systems were present even in the early days of the IC industry, though the term MEMS was not coined until the early 1980s. The defining feature of MEMS is the presence of a mechanical

component in addition to the electronic elements comprising the system. The first such devices were a resonant gate field effect transistor (RGT) (Nathanson and Wickstrom, 1965) and a pressure sensor based on the piezoresistive effect of Si as demonstrated by Kurtz and Goodman (1974) during the period 1961-70. Soon, new manufacturing techniques such as isotropic and anisotropic etching of Si emerged (Waggener et al., 1967), allowing pressure sensor diaphragms and cavities to be built directly into the Si substrate in a single etching step. The period 1970-80 resulted in the demonstration of the first micro-machined accelerometer, the ink-jet printer nozzle, and various other solid-state sensors. Howe (1980) demonstrated the use polycrystalline silicon layers, forming capacitive structures on the surface of a Si substrate. Soon, the first surface micro-machined resonant cantilever gas sensor was demonstrated by Howe and Muller (1986) at Berkley. The ensuing interest in this technology soon led to an industrial and scientific boom, resulting in polysilicon accelerometers, electrostatic motors, and lateral comb drives. A series of conferences held in 1987-88 led to the widespread acceptance of the terms MEMS, micro-systems, and micro-machines in US, Europe and Japan, respectively. By the early to mid 1990s, polysilicon structures were being used to develop integrated accelerometers (Analog Devices; 1993), light modulators and gratings (Silicon Light Machines; 1992), digital mirror display (Texas Instruments; 1993).

With the maturation of this technology and the emergence of high aspect ratio micro-machining methods such as LIGA (Menz, 1992), HEXSIL (Keller and Howe, 1995), soft-LIGA (Sadler et al., 2001), and Deep Reactive Ion Etching (DRIE)(Jansen et al., 2001), MEMS grew closer and closer to their macroscopic counterparts by extending in the third dimension. This development was quite important, since unlike integrated circuits, MEMS are required to perform some sort of mechanical action for which a robust actuator is needed. Interest in applying MEMS to biological and optical applications led to two new terms, “bio-MEMS” and “MOEMS” (Micro-Optical Electro-Mechanical Systems). Numerous foundries were opened in the US (e.g., MCNC and Sandia National Labs) and across the world to provide services to the MEMS community. In 1998-2002, coinciding with the “dot-com” (.com) era of economic boom and bust, many companies invested in optical MEMS for telecommunications and optical switching. Unfortunately, this enthusiasm did not pay out and many companies were forced to close their doors. Since 2000, the research focus has shifted to radio-frequency (RF) MEMS for steerable antennas, switches, and variable RF attenuators and resonators. The interest in bio-MEMS and lab-on-a-chip applications continues to be strong, as is the area of nano-electromechanical systems (NEMS), a term reserved for systems with characteristic lengths below 100 nm.

### 3 Basic MEMS Fabrication Process and Terminology

#### 3.1 Substrates

Since MEMS emerged as a spin-off of well-developed semiconductor processes, the most commonly used substrates for MEMS are semiconductors such as Si, Ge, and GaAs. Due to the need for chemically inert materials, glass, ceramics, and lately even printed circuit boards (Enikov and Lazarov, 2003) have been utilized in the fabrication of MEMS devices. Silicon substrates are the most popular, since a wide range of pro-

cesses and equipment is available for this material. Other commonly used substrates include boro-silicate glasses (Pyrex), alumina, and a range of polymeric materials including polymethyl-methacrylate (PMMA) and poly(dimethylsiloxane) (PDMS) rubber, mostly used in micro-fluidic and biomedical micro-devices.

Silicon, which is a Group IV element, is the most widely used substrate material. Its unit cell can be constructed by starting with a face-centered cubic (FCC) cell and adding four more atoms at locations  $(a/4, a/4, a/4)$ ,  $(3a/4, 3a/4, a/4)$ ,  $(3a/4, a/4, 3a/4)$ , and  $(a/4, 3a/4, 3a/4)$ , where  $a$  is the lattice constant of the original FCC cell. These four atoms form a diamond lattice within the FCC lattice (see Fig. 3(a)). Large single crystals of Si are grown from a melt in a process called Czochralski growth. The process starts with a seed crystal approximately 0.5 cm in diameter, which is brought in contact with a Si melt. Through a slow withdrawal and rotation, a cylindrical boule with diameter up to 300 mm and length reaching 1-2 m is formed. The boule is then sliced and the slices polished to form very smooth substrates (wafers). The crystal orientation and doping type of each wafer are denoted by standard cuts ("flats") on its periphery, as indicated in Figure 4. The following are typical specifications for a starting Si wafer:

- Orientation: (100) or (110)
- Size: 2", 3", 4", 6", 8"
- Thickness: 11-13 mils, 1 mil=1/1000 of an inch=25.4  $\mu\text{m}$
- Dopant type: B, P, As
- Dopant level (resistivity): 3-10  $\Omega\text{-cm}$
- Defects: dislocation density less than 100/cm<sup>2</sup>
- Bow: typically less than 20  $\mu\text{m}$

A thorough substrate cleaning is also required at the beginning of the process to remove any organic films, particulates, native oxides, and metal ion contaminants, and to reform a contamination-free native oxide. Contamination usually occurs during the grinding and polishing process (heavy metals), from human handling, and from other chemicals coming in contact with the wafer or processing equipment. Therefore MEMS, similar to IC chips, are manufactured in clean-room environments, where the number of airborne particles is controlled.

Similar to integrated circuit processing technology, MEMS are built through multiple cycles of material deposition (additive process), patterning (image formation), and pattern transfer (subtractive process). This cycle is illustrated in Figure 5. Electronic circuits typically use 10-18 photolithographic (patterning) steps, while MEMS structures can be usually constructed with fewer steps. These three fundamental processes are described briefly in the following sections.

### 3.2 Photolithography

Photolithography is the core of almost all fabrication process, since this step defines the geometry of the structures used in a micro-device. There are two types of photosensitive materials (photoresists or simply resists): positive and negative (tone) resists. With positive resists, the areas exposed to ultraviolet (UV) light become soluble through a photolysis process occurring in the polymer network. Conversely, negative resists become insoluble (cross-linked) in the areas exposed to UV light. Positive resists

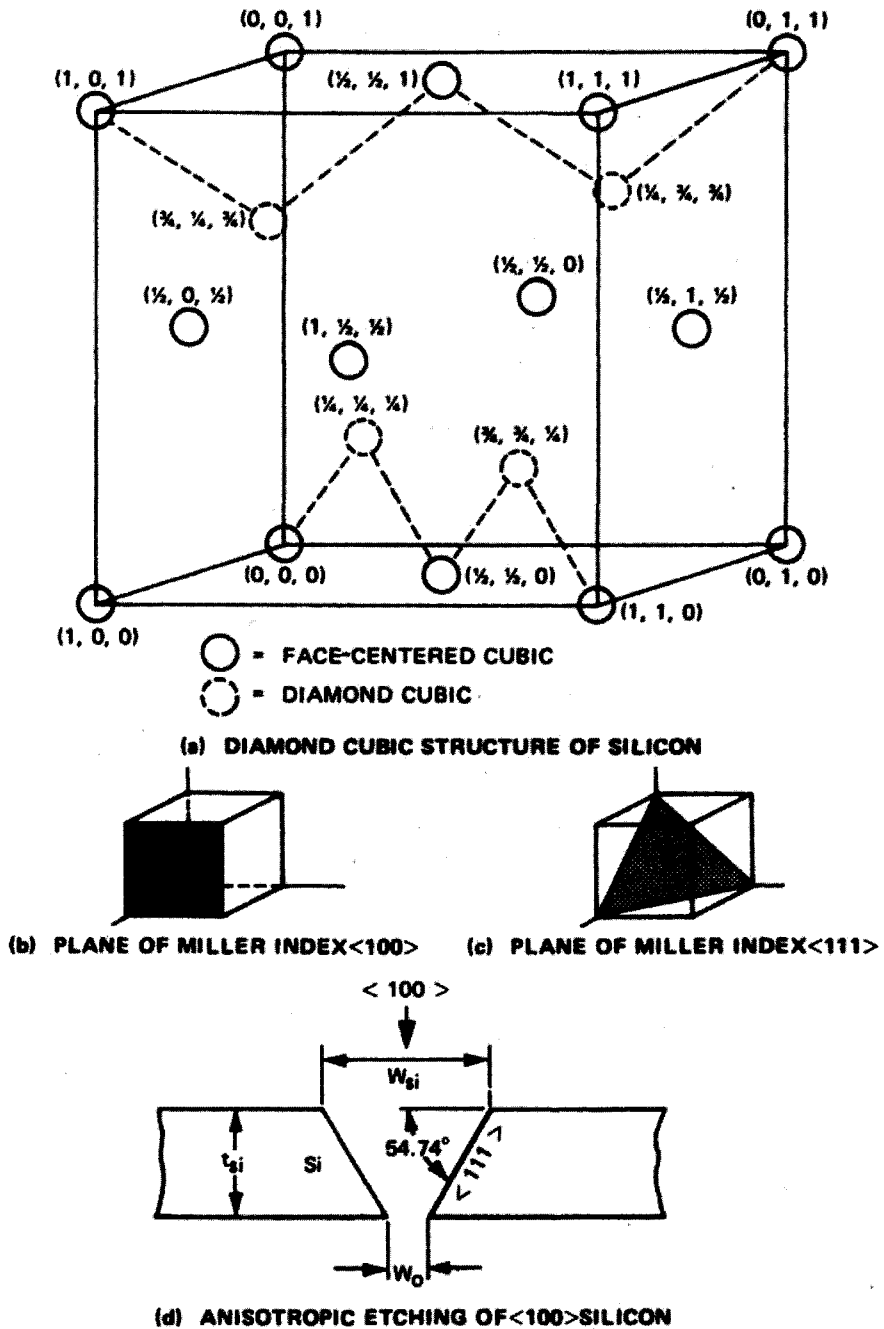


**Figure 3.** (a) Silicon lattice; (b-c) key crystallographic planes; (d) anisotropic etch delineating (111) planes. Reproduced with permission from Brodie and Muray (1992).

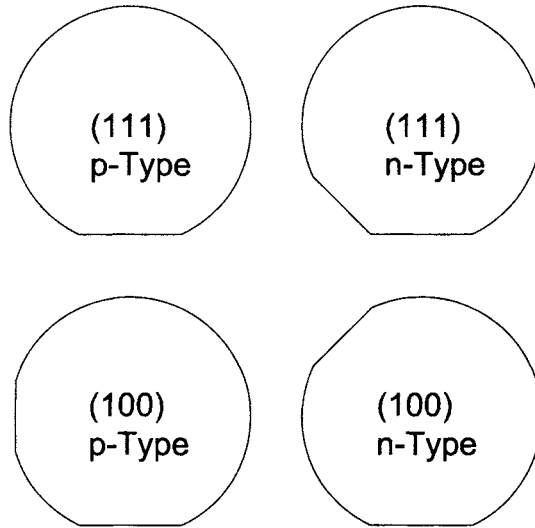


**Figure 4.** Wafer types and flat orientation

are sensitized with diazoquinone (DQ), which is base-insoluble but, when exposed to UV radiation, photolyses and produces carbene, which is then transformed to ketene (using the residual water in the film), and thus becomes soluble in a caustic solution.

Negative resists undergo cross-linking through a photon-initiated radical formation of the azid group, which releases nitrogen.

Differences between positive resist and negative resist pattern formations is shown in Figure 6. As illustrated in the figure, light diffraction and scattering produces wider lines in the negative resist and narrower lines in the positive resist. The following terms are commonly used to characterize the quality of the photolithographic process (ome of these are defined procedurally):

- *Resolution* is the smallest line-width that can be printed reliably under typical variations in the manufacturing conditions.
- *Line-width* is the horizontal distance between the resist-air interface at a given height above the substrate. The defined line-width depends on the method used to measure it. For example, different line-widths will be established though optical, mechanical scanning.
- *Contrast* is the rate of formation or scission of a cross-linked network for negative resists and positive resists, at a constant exposure dose.

The contrast  $\gamma$  can be determined experimentally via measurement of the developed

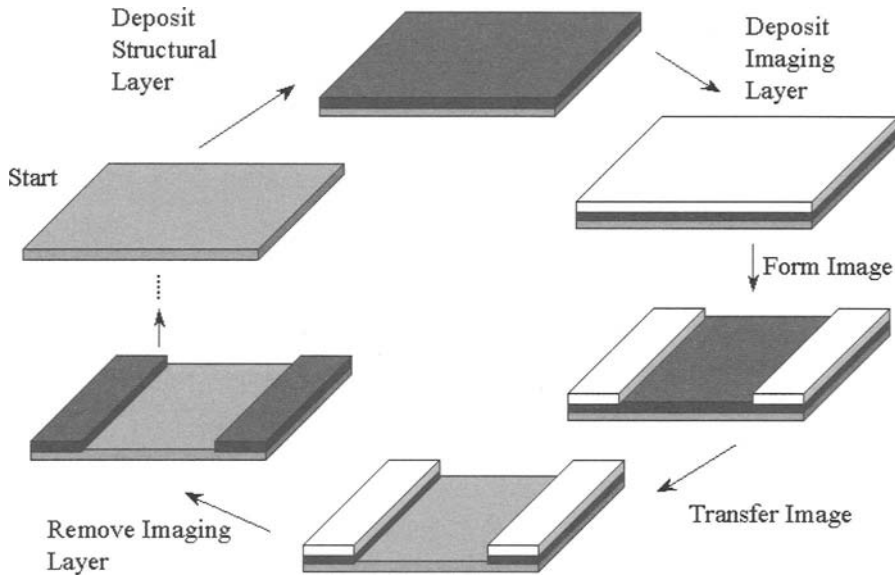


**Figure 5.** MEMS and IC processing cycle.

resist thickness vs. exposure dose (Wolf and Taubert, 2000). For example, for a negative resist the contrast  $\gamma_n$  is determined from

$$\gamma_n = \log_{10}^{-1} \frac{D_0}{D_i}, \quad (3.1)$$

where  $D_i$  is the critical exposure dose under which no cross-linking occurs and  $D_0$  is the extrapolated dose for which complete cross-linking occurs (see Fig. 7). For positive photoresists, the contrast value is determined analogously

$$\gamma_p = \log_{10}^{-1} \frac{D_c}{D_0}, \quad (3.2)$$

where  $D_c$  is the critical exposure dose under which there is always some undeveloped (cross-linked) photoresist and  $D_0$  is the extrapolated dose under which all of the photoresist remains cross-linked. Commonly used positive photoresists have higher contrast values in comparison with negative resists and can therefore produce images with higher resolution. The adhesion to silicon and the chemical resistance of positive resists, however, are somewhat inferior. The main drawback of negative photoresists is their significant swelling during development, which limits the minimum feature size to about 2  $\mu\text{m}$ .

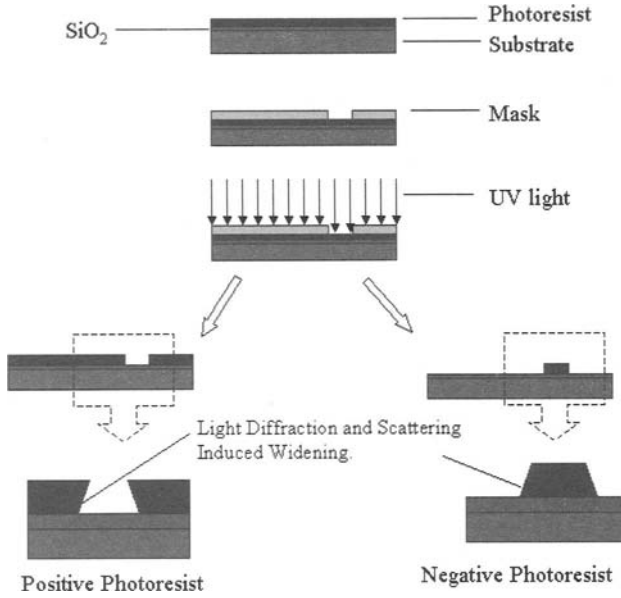


**Figure 6.** Positive and negative resist patterns

Due to light diffraction and scattering, it is clear that the resist thickness is very important in achieving a desired resolution. As a rule of thumb, the minimum feature size cannot be significantly smaller than the thickness of the photoresist. Therefore, methods for producing a uniform film over the entire substrate are needed. Several such techniques are available:

- Spray
- Electrophoretic deposition
- Dip-coating
- Lamination (“dry resists”)
- Spin coating

Among these, the most common is spin-coating, which results in very uniform films. In spin-coating, the substrate is spun at a given rate, allowing centrifugal forces to thin the dispensed solution of photoresist to a film with the desired thickness. This relatively simple process results in a remarkably uniform layer, with sub-micron thickness variations over the surface of a 100-200-cm-diameter wafer. A simple insight into the reasons behind this can be gained from the solution of an axisymmetric flow problem of a Newtonian fluid driven by centrifugal forces. Equating the viscous drag in the radial direction with the centrifugal forces one has

$$\eta \frac{\partial v}{\partial z^2} = -\rho \omega^2 r, \quad (3.3)$$

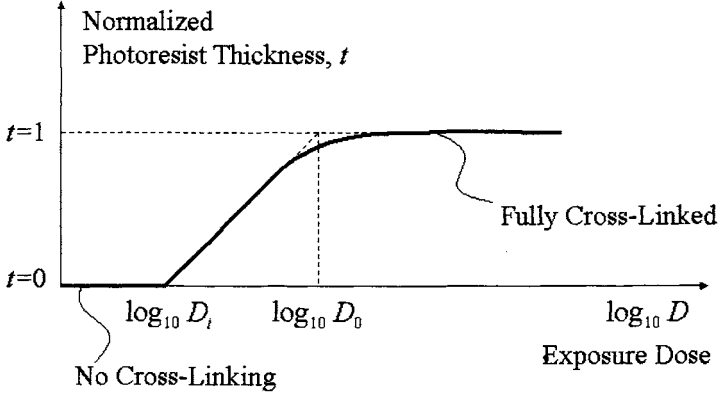


**Figure 7.** Contrast plot of negative photoresist.

where  $\eta$  is the resist viscosity,  $\rho$  its density,  $v$  is the fluid velocity, and  $z$  and  $r$  are the axial and radial coordinates. Simple integration with  $v(z=0) = 0$  and  $\partial v/\partial z(z=h) = 0$  results in

$$v = \frac{\rho\omega^2 r}{\eta} \left[ -\frac{z^2}{2} + hz \right], \quad (3.4)$$

where  $h$  is the thickness of the fluid (photoresist). The total mass of fluid flowing per unit length of a circle with radius  $r$  is

$$q = \int_0^h v(z, r) dz = \frac{\rho\omega^2 r h^3}{\eta 3}. \quad (3.5)$$

Using mass conservation, one can find that the fluid height at a distance  $r$  from the axis of rotation is governed by a simple first-order differential equation

$$\dot{h} = -\frac{1}{r} \frac{\partial}{\partial r} (rq) = -\frac{1}{r} \frac{\partial}{\partial r} \left( \frac{\rho\omega^2 r^2 h^3}{\eta 3} \right) \approx -\frac{2}{3} \frac{\rho\omega^2}{\eta} h^3, \quad (3.6)$$

where the height  $h$  has been assumed independent from the radius  $r$ , which is experimentally observed. Solving Eq. (3.6), one finds that the film thickness is inversely proportional to the square of the angular velocity

$$h(t) = \frac{h_0}{\sqrt{1 + \frac{4}{3} h_0^2 \frac{\rho\omega^2}{\eta} t}}, \quad (3.7)$$

where  $h_0$  is the initial film height. For long times, the height is independent of the initial amount of dispensed liquid  $h_0$  and is given by

$$h^{\text{inf}} = \left( \frac{4}{3} h_0^2 \frac{\rho\omega^2}{\eta} t \right)^{-\frac{1}{2}}, \quad (3.8)$$

which predicts a zero height at infinitely long times. In reality, a finite height is established, which is not equal to the predictions of Eq. (3.8). This is due to solvent evaporation during spinning, which changes the viscosity of the film and arrests the flow after some time. An empirical model describing the residual thickness is given by

$$h^{\text{inf}} = \frac{KC^\beta \eta^\gamma}{\omega^\alpha}, \quad (3.9)$$

where  $K$  is a calibration constant,  $C$  is the polymer concentration in grams/100 ml solution,  $\eta$  is the intrinsic (kinematic) viscosity, and  $\omega$  is the "spin speed" in revolutions per minute (rpm). Meyerhofer (1978) has shown that when the evaporation is accounted for, the value of the exponent  $\alpha$  is approximately 2/3. Typical spin speeds range from 500 rpm up to 7000 rpm, producing films with a thickness of tens of microns down to a fraction of a micron.

A typical photolithography step includes:

- Spin-coating of photoresist at 1000-4000 rpm.
- Pre-exposure bake (soft bake) at 90-100 °C to remove residual solvent in the film;
- UV exposure at 130-170 mJ/cm<sup>2</sup>
- Development 1-5 min
- Post-exposure bake at 110-125°C to remove leftover solvents and make the film more resistive to chemical attacks.

The photolithographic step is almost always preceded by a deposition step, which lays down the layer to be patterned. There are many deposition techniques currently in use in the fabrication of MEMS devices. The main ones used for the deposition of films less than 2-3  $\mu\text{m}$  thick are physical vapor deposition (PVD) and chemical vapor deposition (CVD). Techniques producing thicker layers (above 4-5  $\mu\text{m}$ ) are electrodeposition (electroplating), polymer casting, spray coating, or high-pressure oxidation (HIPOX) of silicon.

### 3.3 Thermal Oxidation of Silicon

Thermally grown  $\text{SiO}_2$  layers are the most important insulator in semiconductor devices. They serve as the gate insulator in CMOS transistors, dielectric in capacitive elements, as well as a masking material for a variety of process steps such as doping and etching. In micro electro-mechanical systems, the silicon dioxide (oxide) serves similar roles. There are many reasons behind the popularity of this dielectric in semiconductor device fabrication, the most important of which is its good electrical properties, ease of film growth, and its superior masking properties. The interested reader is referred to a monograph by Nicollian and Brews (1982) for an extensive discussion on the electrical properties of silicon dioxide and a variety of methods for its characterization.

The silicon dioxide is most commonly deposited via thermal oxidation in high-temperature quartz tubes under the supply of oxygen, steam, and possibly an inert carrier gas such as nitrogen or argon. Typical oxidation temperatures range from 850 °C to about 1272 °C. Figure 8 shows a cross section of the silicon wafer with a thin silicon dioxide film growing on its surface. As illustrated in the figure, the oxidation takes place at the interface between the single-crystal silicon surface and the already grown film,

which requires oxygen to diffuse through the already grown oxide in order to continue the film growth. From a technological point of view, it is important to be able to predict the required time for growing a film with a given thickness. In order to do this, a model based on the diffusion of oxidants (oxygen or water) was developed by Deal and Grove (1965) that allows accurate prediction of the final thickness of the grown film. With the notation from Figure 8, one can set up equilibrium flux conditions for oxygen arriving from the gas phase to the surface, then diffusing through the oxide, and finally reacting with the silicon surface. In the Deal-Grove model, each of these fluxes is related to

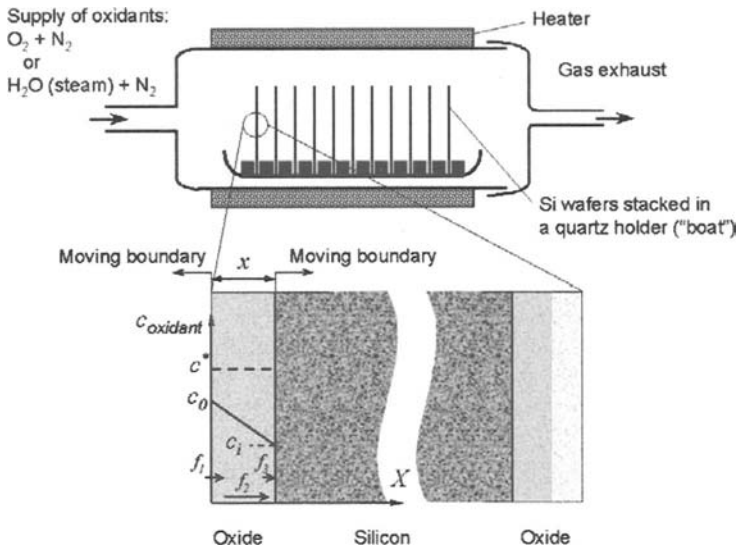


**Figure 8.** Wafer oxidation equipment (upper half); and parameters used in the Deal-Grove's oxidation kinetics model (bottom half).

the concentration of the oxidant diffusing through the silicon oxide. The flux entering the oxide from the gas phase is proportional to the difference between the equilibrium concentration  $c^*$  and the actual surface concentration  $c_0$  at the oxide-air interface

$$f_1 = h(c^* - c_0), \quad (3.10)$$

where  $h$  is the mass transfer coefficient for the air-oxide interface. The equilibrium concentration  $c^*$  is proportional to the external gas pressure through Henry's law

$$c^* = HP, \quad (3.11)$$

where  $P$  is the partial pressure of the oxidant in the chamber and  $h$  is the Henry's law coefficient. Assuming a linear concentration profile, this flux is given by

$$f_2 = \frac{D(c_0 - c_i)}{x}. \quad (3.12)$$

Finally, the oxidant is consumed by the silicon oxidation reaction

$$f_3 = Kc_i, \quad (3.13)$$

where  $K$  is the reaction rate constant. Combining Eqs. (3.10), (3.12), and (3.13) and eliminating the variable  $c_o$  results in

$$c_i = \frac{c^*}{1 + K/h + Kx/D}. \quad (3.14)$$

A differential equation describing the growth of the oxide thickness,  $x(t)$  is derived by using Eq. (3.13), and realizing that the rate of change of the consumption of the oxidant is proportional to the growth rate

$$N_i \frac{dx}{dt} = f_3 = Kc_i = \frac{Kc^*}{1 + K/h + Kx/D}, \quad (3.15)$$

where  $N_i$  is the number of oxidant molecules needed to grow a unit volume of oxide. For  $\text{SiO}_2$ ,  $N_i = 2.2 \times 10^{22}$  molecules/cm<sup>3</sup> (Brodie and Muray, 1992). Integrating Eq. (3.15) between the initial and final oxide thickness  $x_i$  and  $x_o$ , respectively, for the time interval  $[0, t]$  gives

$$x_o^2 + Ax_o = B(t + \tau), \quad (3.16)$$

where

$$\begin{aligned} A &= 2D \left( \frac{1}{h} + \frac{1}{K} \right) \\ B &= \frac{2Dc^*}{N_i} = \frac{2DHP}{N_i} \\ \tau &= \frac{x_i^2 + Ax_i}{B}. \end{aligned} \quad (3.17)$$

The parameter  $\tau$  measures the effect of the initial oxide thickness, which affects the rate of oxidation. Equation (3.16) has one positive root

$$x_o = \frac{A}{2} \left( \sqrt{1 + \frac{t + \tau}{A^2/4B}} - 1 \right). \quad (3.18)$$

There are two growth regimes. For short oxidation times and thin initial oxides ( $t + \tau \ll A^2/4B$ ), the growth is approximately linear

$$x_o \approx \frac{B}{A}(t + \tau). \quad (3.19)$$

It can be noted that  $B/A$  is dependent on the reaction rate  $K$ , but is independent from the diffusion constant. This regime is therefore known as reaction-limited growth. If a longer oxidation is performed and/or there is a significant initial oxide ( $t + \tau \gg A^2/4B$ ), the growth is parabolic

$$x_o \approx \sqrt{B(t + \tau)}. \quad (3.20)$$

In this regime, the growth rate is parabolic and is dependent on  $B$ , which is a function of the diffusion constant, but is independent from the reaction rate. In both cases, the growth coefficients are strongly dependent on the equilibrium concentration  $c^*$  and, through (3.11), on the external pressure. The growth rate can be increased dramatically by increasing the external pressure or the oxidation temperature. Since practical temperature limits are around 1200 °C, oxides beyond 2  $\mu\text{m}$  are grown using high-pressure oxidation (HIPOX) at 10-20 atm. When water vapor (steam) is used instead of oxygen, the growth rate is usually higher due to the higher equilibrium concentration of water,  $c^*$ , in the oxide (higher solubility). This is commonly used in MEMS fabrication, where thick oxides are grown in steam (“wet” oxide) to be used as etch or diffusion masks. When a high-quality oxide is needed, as in the gates of field effect transistors, steam use is avoided to ensure a denser oxide with fewer electrical traps (defects). The parameters  $A$  and  $B$  have an Arrhenius-type dependence on temperature, as well as the nature of the oxidant ( $\text{O}_2$  vs.  $\text{H}_2\text{O}$ ). The Deal-Grove model (Deal and Grove, 1965) does not accurately model the oxide growth for very thin oxides (below 30 nm), where some other oxidation mechanisms appear to be at play. To correct for these effects, a time offset parameter,  $\tau$ , is used to correct for the apparently thin initial oxide when using Eq. (3.19) for thin, dry oxides. Table 1 lists the experimentally determined values for several temperatures and oxidation conditions, along with the values of this empirically established offset parameter.

**Table 1.** Oxidation rate constants, after Deal and Grove (1965).

Temperature [°C]	Wet Oxide		Dry Oxide		
	A [ $\mu\text{m}$ ]	B [ $\mu\text{m}^2/\text{hr}$ ]	A [ $\mu\text{m}$ ]	B [ $\mu\text{m}^2/\text{hr}$ ]	$\tau$ [hr]
920	0.50	0.203	0.235	0.0049	1.4
1000	0.226	0.287	0.165	0.0117	0.37
1100	0.11	0.510	0.090	0.027	0.076

### 3.4 Doping

Doping, one of the most essential processes used in creating integrated circuits, introduces electrically active impurities, resulting in local changes of conductivity and the formation of passive and active devices. In micro-system fabrication, doping is used for similar purposes, as well as to modify the electro-chemical properties of Si. For example, a heavily doped p+ silicon is resistant to alkaline etching and can be used as an electro-chemical etch stop. This process can be utilized to produce Si diaphragms in pressure sensors or the nozzles of inkjet printer-heads (Brodie and Muray, 1992). The process is illustrated in Figure 9.

Pressure-sensitive resistors (piezo-resistors) integrated into the structure can also be fabricated through doping. These resistors are typically used to measure the stress in a diaphragm (pressure sensor) or micro-cantilever force sensors. There are two main methods for introducing impurities into semiconductors: diffusion and ion-implantation.

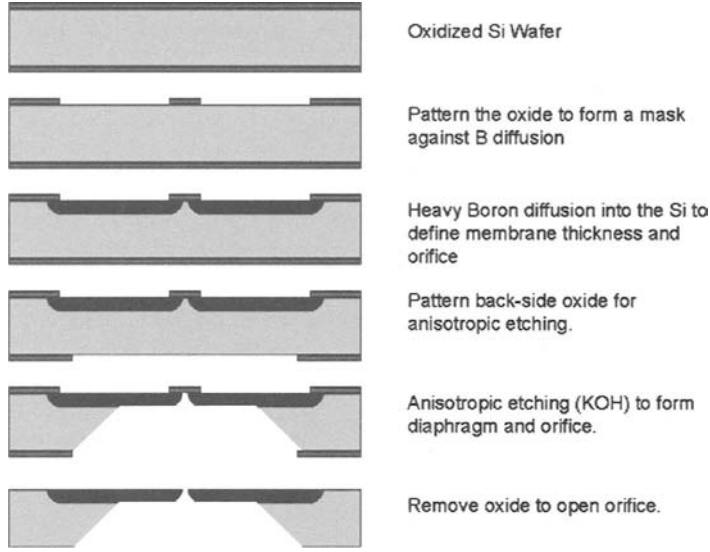


**Figure 9.** Fabrication sequence of a micro-nozzle for a printer-head via heavy (p+) doping, followed by anisotropic etching.

In the case of diffusion, impurities (dopants) are introduced from a solid, gas, or liquid source and then diffused into the substrate in what is known as a classical two-step thermal diffusion process. During the first step (predeposition), the total amount of impurities (dose) is established by maintaining the concentration at the surface at the solid solubility limit. During the second step (drive-in), thermal diffusion under no additional supply of surface impurities re-distributes them into the substrate to establish the desired metallurgical junction depth. During each step, the dopant distribution, the junction depth, and, subsequently, the resistance of the diffused resistor can be determined from the (1D) diffusion equation

$$\frac{\partial c}{\partial t} = D \frac{\partial^2 c}{\partial x^2}, \quad (3.21)$$

where

$$D = D_0 \exp(-E_a/kT) \quad (3.22)$$

is a temperature-dependent diffusion coefficient with activation energy  $E_a$ . Strictly speaking, the parameter  $D_0$  is, in fact, dependent on the impurity type and its concentration. For example, the diffusion coefficient of boron (a p-type dopant) has the form (Runyan and Bean, 1990)

$$D = \left( D^* + D^+ \frac{p}{n_i} \right) \exp(-E_a/kT) = \left( 0.037 + 0.41 \frac{p}{n_i} \right) \exp(-3.46/kT); \quad (\text{cm}^2/\text{s}), \quad (3.23)$$